Deciphering the Ground State of a C 3 -Symmetrical Blatter-type Triradical by CW and pulse EPR Spectroscopy

Athanassios Boudalis, Christos Constantinides, Nicolas Chrysochos, Raanan Carmieli, Gregory Leitus, Andreas Kourtellaris, Daniel Lawson, Panayiotis Koutentis

Deciphering the Ground State of a C_3-Symmetrical Blatter-type Triradical by CW and pulse EPR Spectroscopy

Athanassios K. Boudalis,*[,a] Christos P. Constantinides,*[,b] Nicolas Chrysochos,[c] Raanan Carmieli,[d] Gregory Leitus,[d] Andreas Kourtellaris,[c] Daniel B. Lawson[b] and Panayiotis A. Koutentis[c]

[a] Institut de Chimie de Strasbourg (UMR 7177, CNRS-Unistra), Université de Strasbourg, 4 rue Blaise Pascal, CS 90032, F-67081 Strasbourg, France. Email: bountalis@unistra.fr

[b] Department of Natural Sciences, University of Michigan – Dearborn, 4901 Evergreen Rd, Dearborn, MI 48128, United States

[c] Department of Chemistry, University of Cyprus, P.O. Box 20537, 1678 Nicosia, Cyprus

[d] Department of Chemical Research Support, Weizmann Institute of Science, Rehovot, 76100, Israel

Abstract

3,3',3"-(Benzene-1,3,5-triyl)tris(1-phenyl-1*H*-benzo[*e*][1,2,4]triazin-4-yl) (**1**) is a C_3-symmetrical triradical comprised of three Blatter radical units connected at the 1, 3, 5 positions of a central trimethylenebenzene core. This triradical has an excellent air, moisture, and thermal stability. Single-crystal XRD indicates that triradical **1** adopts a propeller-like geometry with the benzotriazinyl moieties twisted by 174.1(2)° and packs in 1D chains along the *c* axis to form an extensive network of weak intermolecular interactions. Frozen solution continuous wave (CW) EPR spectra and variable-temperature field-sweep echo-detected (FSED) spectra revealed an

intramolecular ferromagnetic exchange within the spin system, supporting a quartet S = 3/2 ground state. DFT calculations further supported these experimental findings.

1. Introduction

High-spin organic radicals are of fundamental interest owing to their potential applications in material sciences [1]. Organic radicals are inherently unstable as nature prefers to pair electrons and maximize bonding in a structure. Nevertheless, there are two main design strategies that can help stabilize unpaired spins in organic molecules: i) steric stabilization whereby bulky groups protect sites of high spin density; and, ii) electronic stabilization (resonance) whereby spin density is either highly delocalized or electronegative elements are introduced in the carbon backbone to offer thermodynamic stability [2]. These design strategies have been successful in the preparation of stable S =1/2 organic radicals. For organic polyradicals with high-spin ground states (S = 1, 3/2, etc.) additional design principles must be followed [3,4]. Spin-containing units, whether atoms or molecules, are usually connected via ferromagnetic coupling units (FCUs) such as trimethylenemethane (TMM) and *m*-benzoquinodimethane (*m*-BQDM) to form high-spin polyradicals [5]. While in closed-shell organic molecules, singlet ground states (S = 0) are separated from low-lying high-spin excited states by tens of kcal mol^{-1}, inverting this large energy gap in favor of a high-spin state for organic polyradicals remains a challenge to this day [6]. The energy gap of the high-spin ground state from the nearest excited state must be in the same order of magnitude as the thermal energy at room temperature (≈ 0.6 kcal mol^{-1}) [7,8]. Furthermore, the high-spin state must be stable and sufficiently populated at room temperature.

We previously reported the synthesis and characterization of a C_3-symmetrical triradical, 3,3',3"-(benzene-1,3,5-triyl)tris(1-phenyl-1*H*-benzo[*e*][1,2,4]triazin-4-yl) (**1**) (Fig. 1), based on 1,3-diphenyl-1,4-dihydrobenzo[*e*][1,2,4]triazin-4-yl (**2**) (aka Blatter's radical) [9]. Several Blatter-based di- and tri-radicals have since been reported in the literature [10-17]. These include mixed Blatter-nitronyl nitroxide and all Blatter di- and tri-radicals wherein the radical units are connected through strategic locations to promote intramolecular ferromagnetic alignment via the spin polarization mechanism. They possess high-spin ground states with robust stability owing to the excellent air, moisture, and thermal stability of Blatter's radical **2** [18-22]. Our extensive synthetic work on this family of radicals has enabled broad access to various derivatives, significantly expanding the structural diversity of the parent radical **2** [23-29]. This has led to many applications in magnetic materials [30-39], photodetection [40,41], liquid crystalline photoconduction [42-45], electroactive building blocks for purely all-organic batteries [46-48], ligands for metal complexes [49-51] and metal-organic frameworks [52], initiators in controlled polymerizations [53-56], Overhauser DNP polarizing agents for high-field MAS-DNP [57] and as pH sensors [58]. These radicals have been shown to have excellent ability to form stable thin films [59,60] which has led to applications in spintronic devices [61-63].

Triradical **1** was designed to connect three Blatter-type radicals onto a 1,3,5-trimethylene-benzene core via their C3 carbons. The latter is a non-disjoint non-Kekulé triradical that acts as a ferromagnetic coupling unit [5]. SOMO orbital calculations for Blatter-type radicals indicate that there is a node on C3 carbons and therefore a question arises as to which is the ground state of triradical **1**. If the nodes on C3 carbons disrupt the communication between the three 'arms', then the three S =1/2 radicals are independent of each other and triradical **1** will have near degenerate high- and low-spin states. However, if the spin polarization mechanism is in effect and there is

sufficient communication between the three radicals then according to Ovchinnikov's rule [4] a high-spin S = 3/2 quartet will be the ground state due to the intramolecular ferromagnetic alignment. Following our reported the synthesis of triradical **1**, Rajca and co-workers [12] commented that triradical **1** is "composed of three S = 1/2 spins that are magnetically independent" and that "this triradical might turn out to be a low-spin (doublet) ground state, very close in energy to the excited quartet". In light of this, and to provide experimental support of the ground state, herein, we report detailed solid-state XRD, solution EPR and computational studies to decipher the ground state of this triradical.

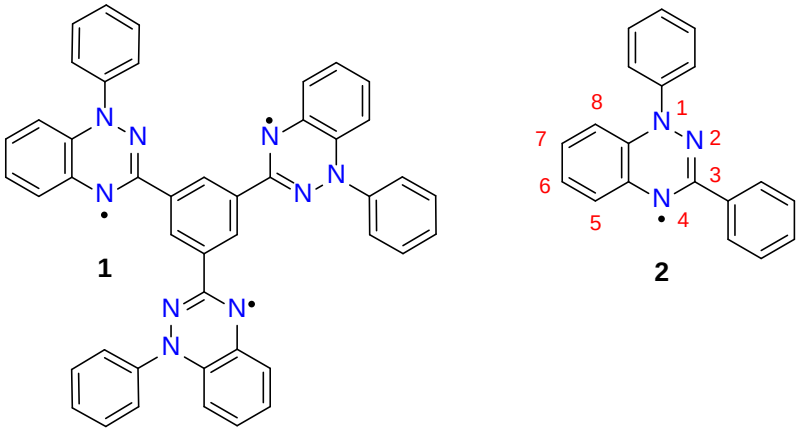

Fig 1. Structure of triradical **1** and Blatter's radical **2**.

2. Experimental

2.1 Single-crystal and powder XRD

Data were collected on an Oxford-Diffraction Supernova diffractometer, equipped with a CCD area detector utilizing Mo-Kα radiation (λ = 0.71073 Å). A suitable crystal was attached to glass fibers using paratone-N oil and transferred to a goniostat where they were cooled for data collection. Unit cell dimensions were determined and refined by using 1617 (4.67° ≤ θ ≤ 28.65°)

reflections. Empirical absorption corrections (multi-scan based on symmetry-related measurements) were applied using CrysAlis RED software [64]. The structures were solved by direct method and refined on F^2 using full-matrix least squares using SHELXL97 [65]. Software packages used: CrysAlis CCD [64] for data collection, CrysAlis RED [64] for cell refinement and data reduction, WINGX for geometric calculations [66], and DIAMOND [67] for molecular graphics. The non-H atoms were treated anisotropically. The hydrogen atoms were placed in calculated, ideal positions and refined as riding on their respective carbon atoms.

Crystal refinement data for triradical 1 (CCDC 1982625)

Dark brown cubes. $C_{45}H_{30}N_9$, M = 696.78, Trigonal, space group $P3$, a = 17.1703(9) Å, b = 17.1703(9) Å, c = 6.8377(4) Å, α = 90°, β = 90°, γ = 120°, V = 1745.81(16) Å^3, Z = 2, T = 100(2) K, ρ_{calcd} = 1.326 g·cm^{-3}, $2\theta_{max}$ = 25°. Refinement of 163 parameters on 2044 independent reflections out of 3962 measured reflections (R_{int} = 0.0267) led to R_1 = 0.0491 [I > 2σ(I)], wR_2 = 0.1518 (all data), and S = 1.163 with the largest difference peak and hole of 0.338 e^{-3} and −0.227 e^{-3}, respectively.

2.2 EPR measurements

EPR spectra of frozen glasses of **1** in 2-Methyltetrahydrofuran (1 mM) were recorded on a Bruker Elexsys E580 spectrometer operating at 9.5 GHz and X-band frequencies (9.5 GHz) equipped with an EN4118X-MD4 resonator at temperature range of 5 K-110 K. The temperature was controlled by an Oxford Instruments CF935 continuous flow cryostat using liquid He. Field-sweep echo-detected (FS-ED) EPR spectra were recorded using the two-pulse echo sequence (π/2-τ-π-τ-*echo*) where the echo intensity is measured as a function of the magnetic field. The microwave pulse lengths, π/2 and π were 10 and 20 ns, respectively and the time interval between the pulses, τ, was 200 ns. The two-pulse ESEEM sequence, π/2-τ-π-τ-echo, was

employed with a two-step phase cycle. The measurements were carried out at a magnetic field where the echo intensity is maximum, and the length of the $\pi/2$ and π microwave (MW) pulses were 12 ns and 24 ns, respectively. The pulse interval τ was selected to be 100 ns with a 12 ns increment. For measuring T_1 the inversion recovery sequence, π-T_d-$\pi/2$-τ-π-τ-echo, was employed with a two-step phase cycle. The measurements were carried out at a magnetic field where the echo intensity is maximum, and the length of the $\pi/2$ and π microwave (MW) pulses were 12 ns and 24 ns, respectively. The pulse interval τ was selected to be 200 ns and T_d was started from 400 ns and increased with a 1600 ns increment.

The IR trace was fitted to a stretched exponential decay law $M(t) = M_0 e^{(-t/T_1)^\beta}$. For the echo decay (ED) traces, the presence of three peaks in their FT spectra, characteristic of ^{1}H, and ^{2}H and double ^{2}H modulation frequencies, required the additional consideration of three modulations, at frequencies ($f_{1\text{-}3}$), each decaying with a characteristic time ($b_{1\text{-}3}$). Various tests determined that the exponential decay obeyed to a stretched exponential process. The relaxation law was:

$$M(2\tau) = M_0 e^{(-2\tau/T_M)^\beta} \left(1 + \sum_{i=1}^{3} k_i e^{-2\tau/b_i} \cos(4\pi f_i \tau + \varphi_i) \right)$$

Fourier transforms were carried out on ED traces after subtraction of the exponential decay background, zero-filling and apodization to a Hamming window function.

Spectra fits to CW spectra were carried out with *Easyspin* v. 6.0 [68] using home-written functions.

2.3 Computational methodology

Full optimization for the doublet and quartet states of triradical **1** were carried using the UB3LYP method [69-72] that performs well for Blatter type radicals [30-39]. Basis sets used in this work included the standard Pople basis sets including the 6-31g(d) and 6-311+G(2d,p) basis sets along with the SVP and TZVP Ahlrichs [73] def2 basis sets. All calculations were performed with Gaussian16 [74] using the University of Michigan's Greatlakes cluster. To estimate the intramolecular exchange-coupling constants ($J_{intra,comp}$) we use the magnetic Heisenberg–Dirac–Van Vleck Hamiltonian for three electrons in a symmetric three center triradical molecular system which can be written as

$$\widehat{H}_{intra} = -\left(J_{12}\ \cdot \hat{S}_1 \cdot \hat{S}_2 + J_{23}\ \cdot \hat{S}_2 \cdot \hat{S}_3 + J_{13}\ \cdot \hat{S}_1 \cdot \hat{S}_3\right)$$

Where J_{ij} is the intramolecular exchange-coupling constants between nearest neighbor spin centers and $\hat{S}_i$ are the spin operators for the three spin sites. As written $\widehat{H}_{intra}$ can be applied to a linear molecular system with spins evenly separated or to a triangular molecular system where the spins are located at the corners of an isosceles triangle [5]. These intramolecular magnetic interactions produce two doublets and one quartet energies [75]. As in this case, the equilateral triangular molecular symmetry reduces the exchange-coupling constants to $J_{intra} = J_1 = J_2 = J_3$ and the resulting energies of the two degenerate doublet states, E_{D}, and one quartet energies, E_{Q}, can be written as [76]:

$$E_{\mathrm{D}} = +{}^{3}/_{4} \cdot J_{intra}$$

$$E_{\mathrm{Q}} = -{}^{3}/_{4} \cdot J_{intra}$$

Computationally, the energy of each magnetic exchange interaction between each spin center is represented as the exchange coupling constant mapped from the energies of the calculated doublet and quartet states. $J_{intra,comp}$ is evaluated from the unprojected formula where

$$J_{intra,comp} = +\tfrac{2}{3}\left(E_{\mathrm{Q}} - E_{\mathrm{D}}\right)$$

According to $\widehat{H}_{intra}$, a positive value of the exchange coupling constant *J* indicates a ferromagnetic interaction between S_i and S_j whereas a negative exchange coupling constant corresponds to an antiferromagnetic interaction between spin centers.

3. Results and Discussion

Triradical **1** was previously prepared in a two-step reaction sequence [9]. 1-(2-Nitrophenyl)-1-phenylhydrazine was condensed with 1,3,5-benzenetricarbonyl trichloride to form the intermediate tris(2-nitrophenyl)-triphenylbenzene-1,3,5-tricarbohydrazide which upon an *in situ* cyclodehydration followed by alkali treatment afforded triradical **1** as black needles in an overall yield of 58%. A variety of techniques were previously used to characterize triradical **1** and the results are summarized here. Differential Scanning Calorimetry (DSC) studies showed that triradical **1** has a significantly higher stability that Blatter radical **2** with a thermal decomposition onset at 312.8 °C and peak max at 314.1 °C and no prior melting point. The UV–vis spectrum of triradical **1** had almost identical absorptions to that of Blatter's radical **2** in terms of peak wavelengths, however, it exhibited almost 2–2.5× higher absorbance. Cyclic voltammetry measurements showed a fully reversible reduction at $E_{1/2}^{red}$ −0.819 V vs SCE and a fully reversible oxidation process at $E_{1/2}^{ox}$ 0.385 V vs SCE, which remained stable after 10 continuous cycles. A broad EPR signal was observed with no detailed structure and hfcc values for the N1 (~2.58 G), N2 (~2.56 G) and N4 (~2.52 G) were similar due to inhomogeneous line broadening.

These data pointed inconclusively to the independence of each triazinyl radical moiety, *i.e*., their identical behavior attributed to little to no spin-spin coupling between them.

From here on, we describe efforts to establish unambiguously the ground state of triradical **1**. We have obtained the structure of triradical **1** (Fig. 2) from single X–ray quality crystals grown by a slow diffusion of *n*-pentane into a chlorobenzene solution of radical **1**. Triradical **1** crystallizes in the trigonal *P*3 space group with one third of the triradical in the asymmetric unit (*i.e.* one benzotriazinyl moiety) and two molecules within the cell. Triradical **1** is nonplanar and adopts a shallow concave form with the benzotriazinyl C7 atoms 0.719 Å above the central benzene plane. The benzotriazinyl moieties twist in a propeller-like geometry by 174.1(2)° (torsion angle of N1-C3-C4-C5) and the dihedral angle of the central and triazinyl planes is 7.0(4)°. The N-phenyls twist out of the benzotriazinyl plane by 42.1(3)° (torsion angle of C15-C10-N2-N1) and the dihedral angle of the N-phenyl plane and the triazinyl plane is 47.6(1)°. No intramolecular interactions are observed.

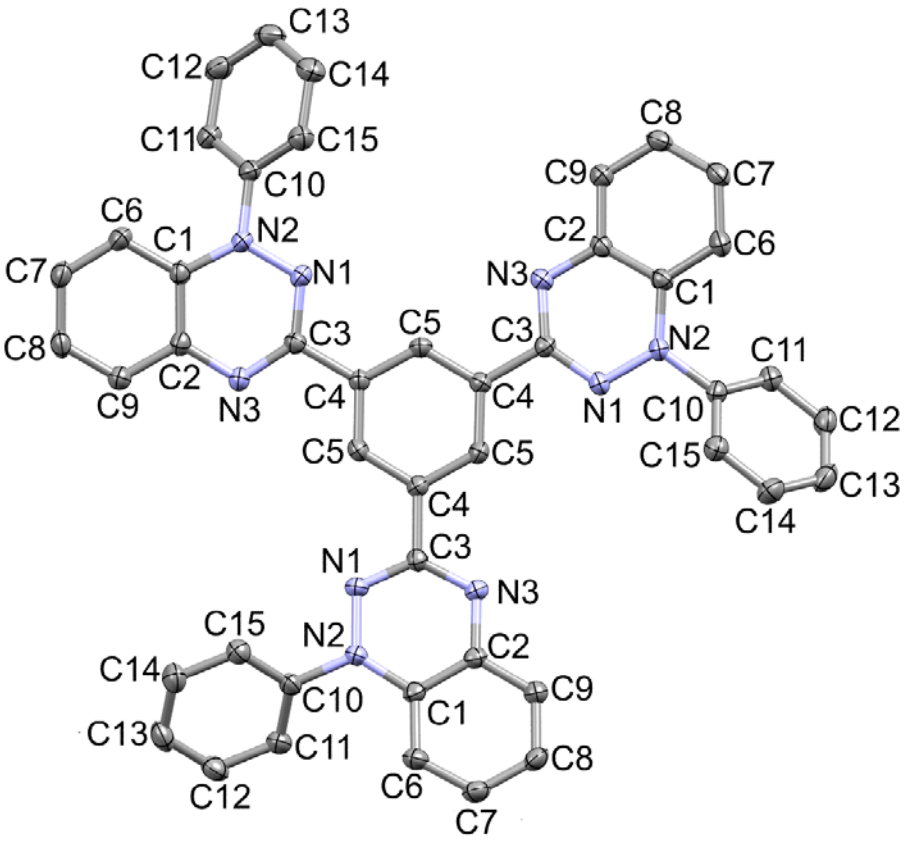

Fig 2. Thermal ellipsoid view of triradical **1** (CCDC 1982625). Crystallographic numbering shown. 50% Probability ellipsoids. Hydrogens omitted for clarity.

Molecules of triradical **1** form one dimensional (1D) chains along the *c* axis (Fig. 3). There are two symmetry operations in the crystal structure of triradical **1**: Two three-fold rotation axis (*-y*, *x-y*, *x* and *-x+y*, *-x*, *z*) with direction [0,0,1] at 0,0,*z* and two three-fold rotoinversion axis (*y*, *-x+y*, *-z* and *x-y*, *x*, *-z*) with direction [0,0,1] at 0,0,*z* and inversion at [0,0,0].

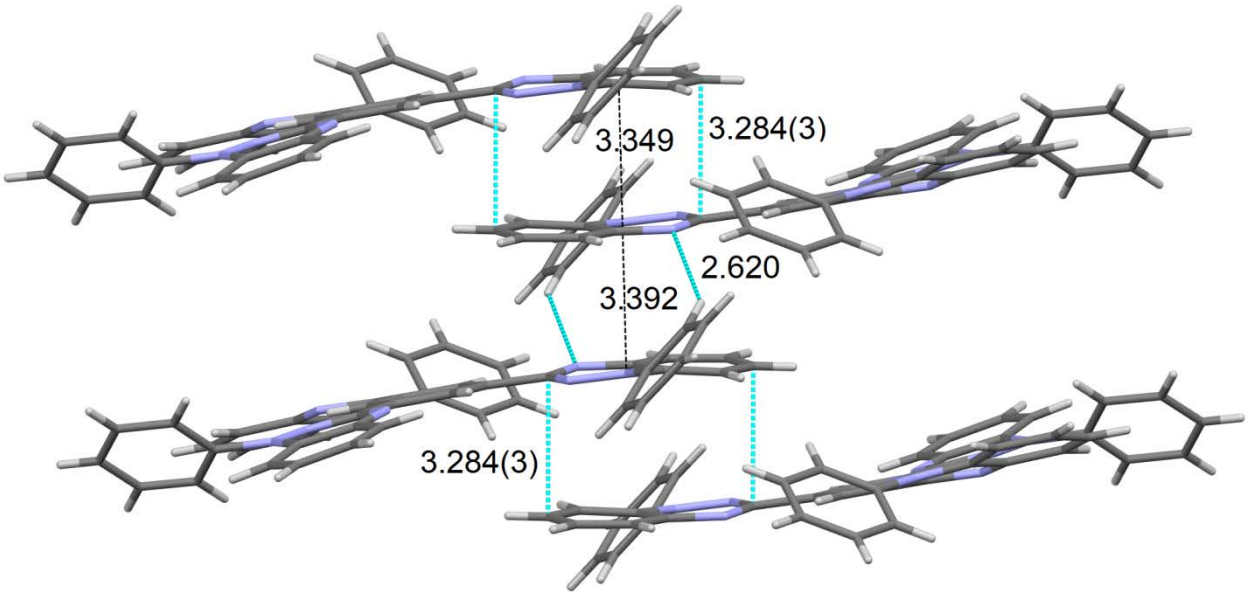

Fig 3. One of the three equivalent supramolecular 1D chains of triradical **1** depicted along the *c* axis showing the alternative distances (Å) forming the radical pairs inside the chain and the closest intermolecular contacts.

Around the central 1,3,5-substituted arene the three benzotriazinyl moieties form identical 1D chains along the *c* axis. The radicals inside these chains are alternatively spaced by 3.392 and 3.349 Å (Fig. 3). This gives rise to two distinct dimers: The opposing molecules separated by 3.392 Å adopt a convex to convex relative orientation and are connected via a 3.419(3) Å [N3···H11-C11 ∠ 144.2°] close contact between the N3 atom of one molecule and the C11 atom of the N-phenyl moiety of the opposing molecule. In contrast, the opposing molecules in the chain separated by 3.349 Å adopt a concave to concave relative orientation and show a 3.284(3) Å close contact between the C3 atom of one molecule and the C7 atom of the benzotriazinyl moiety of the opposing molecule (Fig. 3). Each arm of the triradical **1** interacts with a different molecule, which helps establish an extended network of weak interactions.

The polycrystalline sample used in our studies was examined for phase purity. A comparison (Fig. 4) of the powder XRD diffraction pattern of our sample measured at 300K match well the pattern calculated by the single-crystal structure at 100K.

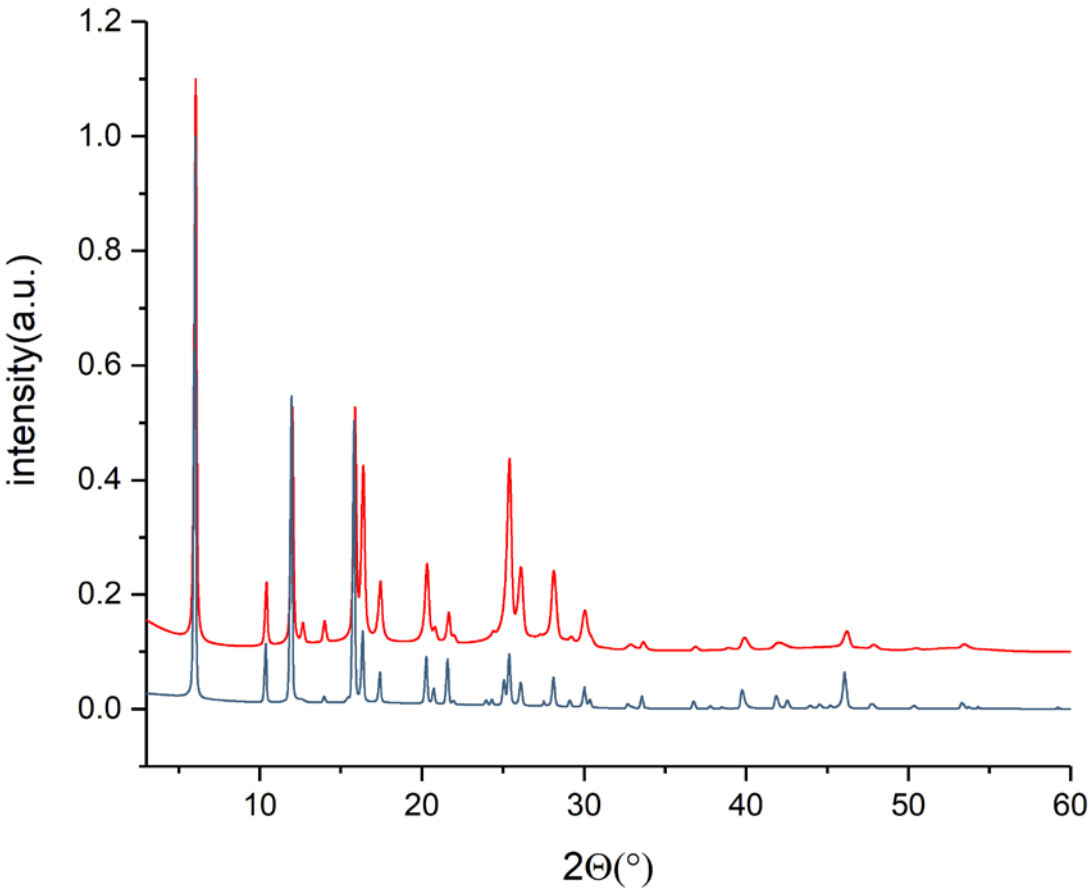

Fig 4. A comparison of the experimental powder X-ray diffraction pattern at 300 K (red) and the calculated one from the single crystal X-ray structure at 100 K.

To assess the magnetic ground state of the individual molecules, solution studies were preferred to avoid intermolecular interactions that would mask the intramolecular ones, as is often the case in organic radicals [1,2,5,6].

CW EPR spectra in frozen 2-Methyltetrahydrofuran at 110 K revealed a pattern typical of a zero-field split system (Fig. 4). Preliminary fits were carried out on a spectrum collected at a

0.65 mW microwave power to better highlight all the resonances and allow a determination of the spin Hamiltonian parameters.

Fitting this to a S = 3/2 spin with axial magnetic anisotropy yielded excellent results demonstrating the presence of a thermally populated S = 3/2 state. The line shapes required the introduction of a small strain in $g_{\perp}$. Best-fit parameters were $g_{3/2\|}$ = 2.0033, $g_{3/2\perp}$ = 2.0046, $\sigma g_{3/2\perp}$ = 0.0098, D = 0.00286 cm^{-1}, σ_G = 0.020 mT, σ_L = 0.48 mT.

To demonstrate the origin of this zfs, we carried out fits to these data using a model considering the dipolar interactions between three S = 1/2 spins. Indeed, dipolar interactions can induce magnetic anisotropy even in systems comprising just S_i = 1/2 spins, thus characterized by absence of single-ion zfs [77]. Based on such a full multispin Hamiltonian, Easyspin builds the associated matrix and computes the energies of the magnetic levels by diagonalization. Boltzmann population analysis at the experimental temperature and magnetic fields is taken into account when calculating the intensities of various EPR spectral resonances, allowing a qualitative estimate of the J coupling.

In the absence of hyperfine splittings, and in a spin system with identical g-values [78], the presence of exchange interactions is not expected to influence the resonance positions spectra, we therefore carried out such preliminary fits considering J_{ij} = 0. Best-fit parameters were $g_{i\|}$ = 2.0034, $g_{i\perp}$ = 2.0046, $\sigma g_{i\perp}$ = 0.0131, r_{ij} = 7.72 Å (i, j = 1-3), σ_G = 0.026 mT, σ_L = 0.43 mT.

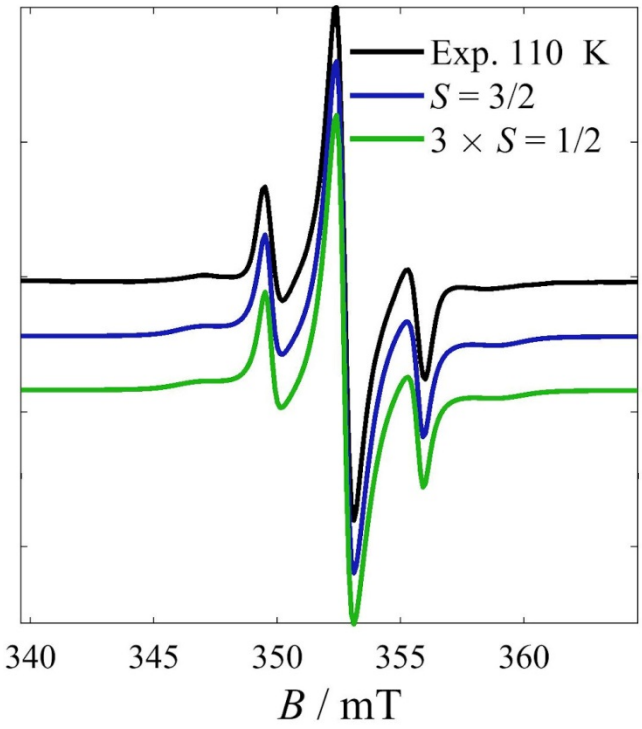

Fig 5. Solution CW EPR spectrum of triradical **1** and fits to two models: a S = 3/2 giant spin with zfs (blue line) and three S_i = 1/2 spins interacting through dipolar interactions. Experimental parameters: f_{MW} = 9.803255 GHz, P_{MW} = 0.65 mW, B_{mod} = 0.1 mT_{pp}.

The two fits yield very close results, including the g-values. The practically identical values of the main elements of the global and local g-tensors indicates that the two reference frames are collinear, *i.e.*, the local g_z axes are parallel to the molecular z-axis; normal to the plane of the central ring. We also note that fits yield $g_{i||} < g_{i\perp}$, in apparent contrast to the previously derived values for the parent monoradical [38]. We are currently unsure of the reasons of this inversion. That these are frozen solution data may introduce important uncertainties in the derived g-values.

The fitted distances are in close, albeit not perfect, agreement with the interatomic distances between spin-bearing atoms N3 (6.360 Å). The slightly larger fitted distance may indicate a small delocalization of the spin density toward carbon atom C2, and/or the interplay of conformational changes through rotation of the side-groups around bond C3-C4. Another possibility, the presence of anisotropic (or "pseudo-dipolar") exchange interactions, whose effects are added to those of the dipolar interactions, is not considered plausible as its physical origins are the spin-orbit coupling effects, which are typically most pronounced in the case of metal ions.

While information on the exchange couplings could not be obtained by the resonance positions, such information might eventually be obtained by their relative intensities. Indeed, the relative energies of the singlet and quartet states is expected to influence the relative intensities of the central and lateral resonances. Indeed, the central resonance is a sum of the $M_S = -1/2 \rightarrow +1/2$ transitions, both within the quartet and within the two doublets, whereas the lateral resonances are only due to the $M_S = -3/2 \rightarrow -1/2$ and $+1/2 \rightarrow +3/2$ transitions within the quartet. Thus, these latter will be relatively enhanced in intensity in the case of a FM coupling, which would make the quartet the ground state.

To assess this, fits were carried out on a spectrum collected at 0.21 μW at 110 K, to minimize any risk of saturation that might distort the spectral intensities. Initial tests demonstrated that fits to such a model were sensitive enough for a qualitative assessment of the sign of J, but not for its quantitative determination. While all fits converged to a FM coupling, the precise J_{ij} value depended on the fitting intervals. In Fig. 6, we present fits with J_{ij} (i, j = 1-3) values fixed to +100 and –100 cm^{-1} ($-J_{ij}S_iS_j$ formalism). These show that the strong FM coupling better reproduced the relative intensities of the two resonances. Moreover, the effects of a moderate FM

coupling were assessed, by carrying out fits with J values fixed to ±3 cm^{-1}. These values were selected based on DFT calculations and analysis of the spin-lattice relaxation times (see below), but also to avoid numerical artifacts produced close to perfect frustration (J = 0). These are practically indistinguishable, and both demonstrate a distinctly lower agreement with the experimental spectrum compared to the J = +100 cm^{-1} fit. While these fits cannot quantitatively determine the J value, on a qualitative level they indicate the presence of FM interactions sufficiently strong to be clearly discerned in the spectra.

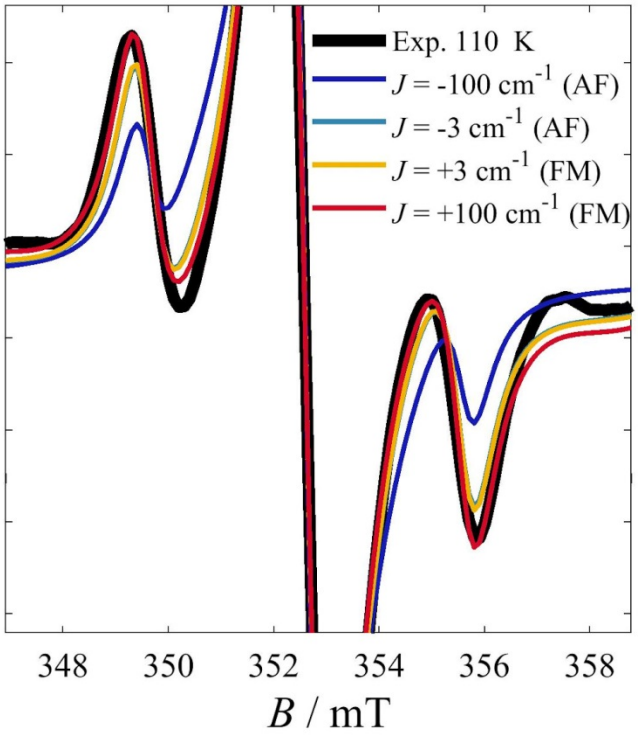

Fig. 6. Zoom of the lateral resonances of **1** at 110 K, showing fits with J_{ij} (i, j = 1-3) values fixed to +100, +3, –3 and –100 cm^{-1}. The spectra are normalized to the central resonance. Experimental parameters: f_{MW} = 9.80009 GHz, P_{MW} = 0.207 μW, B_{mod} = 0.1 mT_{pp}.

To further confirm that the quartet is the ground state, we considered variable-temperature EPR spectroscopy studies in solution as the ideal choice. Indeed, SQUID susceptometry in the

solid state might be dominated by intermolecular interactions which would mask the intramolecular ones [30-39].

Preliminary attempts to address the question through variable-temperature CW EPR spectroscopy were complicated by the appearance of asymmetric derivative spectra which was attributed to passage effects [79,80]. In fact, these are quite common in molecules with relatively slow spin-lattice relaxation and require particular care to remove (such as low MW powers, small modulation frequencies, slow scans), thus complicating the quantitative comparison of variable-temperature data. In the presence of such effects, double integration is particularly imprecise, since small asymmetries in the derivative spectrum are translated in “absorption” spectra with severely distorted baselines. These require corrections that affect the quantification during the second integration in an unpredictable manner.

To circumvent these complications, we undertook pulsed EPR spectroscopy, which directly yields “absorption” field-swept spectra, while also allowing us to monitor the spin-lattice relaxation time at different temperatures to select shot repetition times (SRTs) of appropriate length to assure full relaxation of the magnetization. Preliminary field-sweep echo-detected (FSED) spectra corresponded perfectly to those derived from CW EPR spectroscopy (Fig. 5).

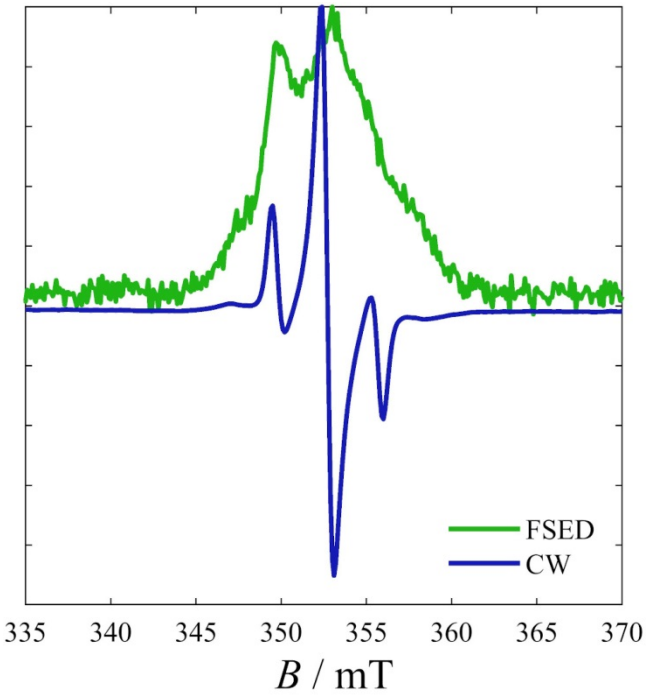

Fig 7. CW EPR and FSED spectra of **1** at 100 K. Experimental conditions. FSED: f_{pEPR} = 9.79866 GHz; CW: f_{CW} = 9.80326 GHz, P_{MW} = 0.65 mW, B_{mod} = 0.1 mT_{pp}.

The spin-lattice relaxation time (T_1) was characterized by inversion recovery (IR) experiments (Fig. 6 and Table 1) at each temperature to select an appropriate SRT for the subsequent pulse EPR studies (SRT > $5T_1$). Echo decay experiments (Fig. 7) were also carried out to assess the phase-memory time of the spin system and select an appropriate interpulse delay for FSED experiments.

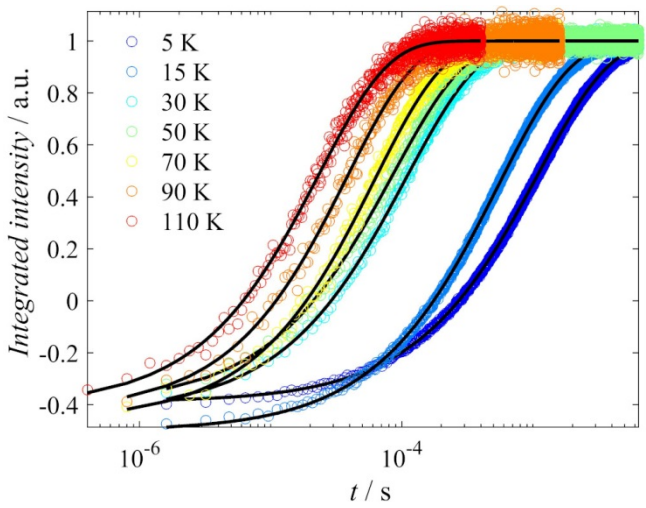

Fig. 8. IR traces at the spectral maximum of **1** (350 mT) recorded at various temperatures, fitted to stretched exponential relaxation law (black lines).

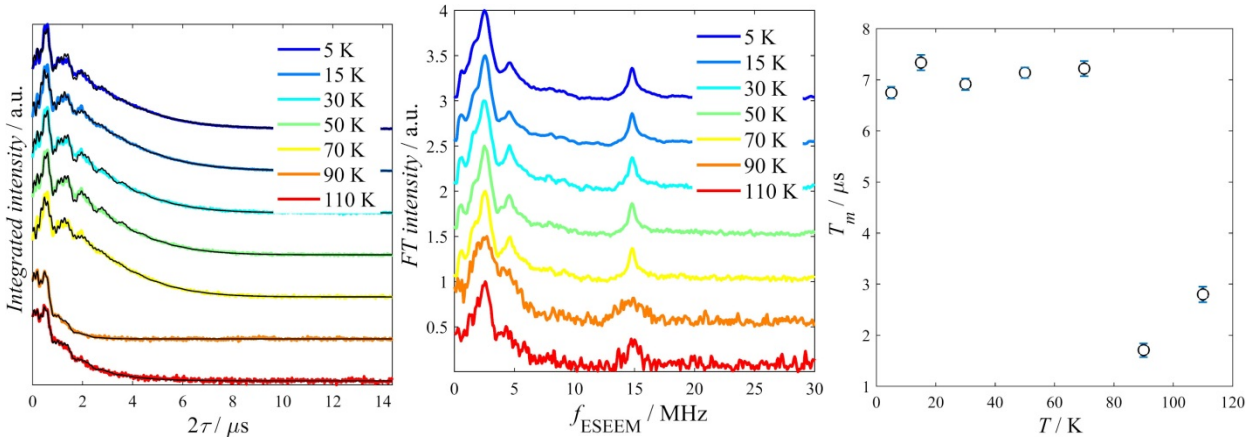

Fig. 9. Left: Hahn echo decay traces at the spectral maximum of triradical **1** (350 mT) recorded at variable temperatures and fitted to a stretched exponential decay modulated by three oscillations of different frequencies. **Middle:** ESEEM FT spectra. **Right:** Best-fit values of T_M times with error bars corresponding to 95% confidence intervals.

Table 1. Best-fit parameters for T_1 and T_M times and their corresponding stretch parameters. Numbers in parentheses indicate the 95% confidence intervals.

T (K)	350 mT		353 mT		350 mT		353 mT	
	T_1 (ms)	β_{T1}	T_1 (ms)	β_{T1}	T_M (μs)	β_{TM}	T_M (μs)	β_{TM}
5	1.098(4)	0.796(4)	1.306(2)	0.798(2)	6.8(1)	1.49(5)	5.91(6)	1.53(3)
15	0.549(3)	0.785(4)	0.671(2)	0.781(2)	7.5(1)	1.64(5)	5.96(6)	1.57(3)
30	0.108(3)	0.77(1)	0.130(2)	0.726(9)	7.0(1)	1.64(6)	5.57(8)	1.56(4)
50	0.085(3)	0.78(2)	0.099(2)	0.73(1)	7.2(1)	1.70(5)	5.89(8)	1.66(5)
70	0.062(2)	0.81(2)	0.073(1)	0.76(1)	7.3(1)	1.76(6)	6.2(1)	1.48(7)
90	0.038(2)	0.83(5)	0.044(2)	0.77(2)	1.7(1)	1.3(1)	2.1(1)	1 (limit)
110	0.023(2)	0.83(4)	0.027(1)	0.75(2)	2.8(1)	1.07(6)	3.8(8)	1.0(2)

Variable-temperature FSED spectra (Fig. 8) were collected, and integrated to derive their intensity *I*. The $I \times T$ products were plotted as a function of temperature. Unfortunately, after correction for the experimental parameters (number of scans, video gain, shots per point), no clear trend was observed for the data.

We have used DFT calculations to further support the experimental results from the CW EPR and FSED spectroscopy. The ground state of triradical **1** was determined computationally using the energies of the doublet and quartet states (Table 2) calculated from full optimizations at the UB3LYP level and using four basis sets 6-31g(d), 6-311+g(2p,d), def2-SVP and def2-TZVP. All basis sets provide similar doublet-quartet splittings ranging 0.117 – 0.124 kcal mol^{-1} in favor of a quartet ground state (Table 2).

The calculations indicate that there is a ferromagnetic alignment of the three unpaired electrons within the triradical molecule. The intramolecular exchange coupling constant, J_{intra}, was calculated to be 2.73 cm^{-1} with the smallest basis set of 6-31g(d) and 2.89 $cm^{-1}$with the

largest basis or the def2-TZVP. The remaining basis sets including the 6-311+g(2d,p) and the def2-SVP give a J of 2.68 cm^{-1} and 2.85 cm^{-1}, respectively. The range in the computed J values is 0.16 cm^{-1} showing very little change with respect to basis.

Table 2. UB3LYP doublet energies, E_D (au), quartet energies, E_Q (au), the doublet-quartet splitting energy (ΔE_{DQ}) of triradical **1** (kcal mol^{-1}), and the computed exchange-coupling constant $J_{intra,comp}$ (cm^{-1}).

Basis Set	E_D (au)	E_Q (au)	ΔE_{DQ} (kcal mol^{-1})	$J_{intra,comp}$ (cm^{-1})
6-31g(d)	-2224.875469	-2224.875656	0.117	2.73
6-311+g(2p,d)	-2225.513669	-2225.513864	0.122	2.86
def2-SVP	-2223.222689	-2223.222883	0.122	2.85
def2-TZVP	-2225.711158	-2225.711355	0.124	2.89

Conclusions

SOMO orbital calculations for Blatter-type radicals indicate that there is a node on C3 carbons [30-39]. At a first glance the SOMO orbital calculations for triradical **1** (Fig. 9) indicate localization of spin in each 1,2,4-benzo[*e*]triazin-4-yl moiety and a nodal carbon connecting the arms directly to the 1,3,5-trimethylenebenzene core. However, the spin density distribution (Fig. 10) shows extensive spin delocalization over the central core and effective communication between each radical unit.

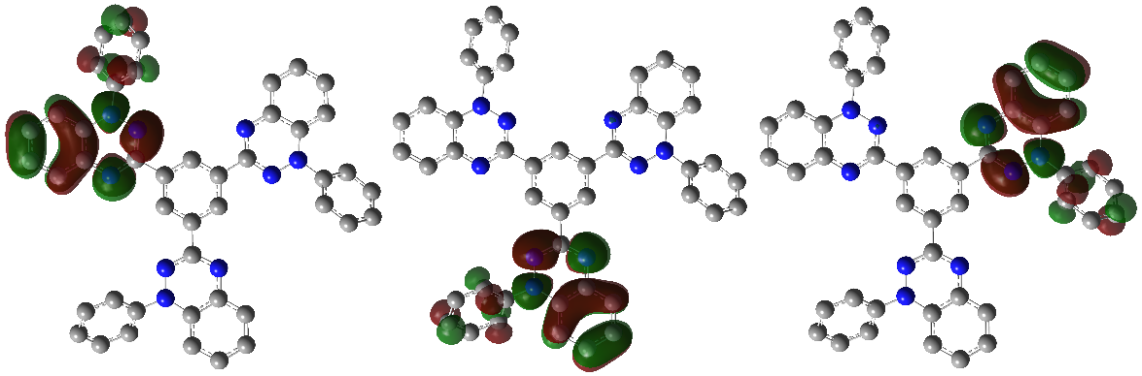

Fig 10. The three degenerate SOMO molecular orbitals ($E_{SOMO(1-3)}$ = −4.920 eV) of the quartet ground state of triradical **2** as calculated with DFT UB3LYP/6-31G(2d,p).

The spin polarization mechanism is in effect and ~~sufficient~~ communication exists between the three radicals. This is supported by variable-temperature FSED spectroscopy which suggests ferromagnetic exchange within the spin system, leading to a quartet ground state. DFT calculations agree with the experimental EPR data and show that the quartet state is more stable than the doublet state by *ca*. 0.122 kcal mol^{-1}. Our data show that despite the anticipation that triradical **1** is "composed of three S = 1/2 spins that are magnetically independent" [12] the radical units do communicate with each other and align in a ferromagnetic manner.

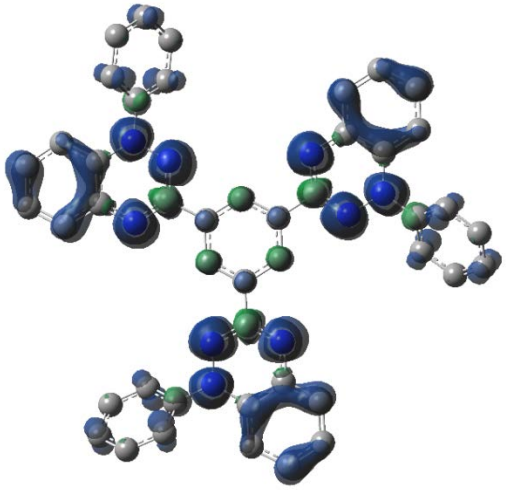

Fig 11. Spin delocalization of triradical **1** calculated at the UB3LYP/6-31G(2d,p) level of theory.

Declaration of competing interest

The authors declare that they have no known competing financial interests or personal relationships that could have appeared to influence the work reported in this paper.

Acknowledgements

C. P. Constantinides thanks the University of Michigan-Dearborn for an UM-Dearborn Scholars award. P. A. Koutentis thanks the A. G. Leventis Foundation for helping to establish the NMR facility at the University of Cyprus, the Cyprus Research Promotion Foundation and the following organizations and companies in Cyprus for generous donations of chemicals and glassware: the State General Laboratory, the Agricultural Research Institute, the Ministry of Agriculture, MedoChemie Ltd., Medisell Ltd., Biotronics Ltd.

References

1. R. G. Hicks (Ed.), Stable Radicals: Fundamentals and Applied Aspects of Odd-Electron Compounds, John Wiley & Sons Ltd, Wiltshire, 2010.
2. R. G. Hicks, What's new in stable radical chemistry?, Org. Biomol. Chem. 5 (2007) 1321-1338.
3. W. T. Borden, E. R. Davidson, Effects of electron repulsion in conjugated hydrocarbon diradicals, J. Am. Chem. Soc. 99 (1977) 4587-4594.

4. A. A. Ovchinnikov, Multiplicity of the ground state of large alternant organic molecules with conjugated bonds, Theor. Chim. Acta 47 (1978) 297-304.
5. A. Rajca, Organic Diradicals and Polyradicals: From Spin Coupling to Magnetism?, Chem. Rev. 94 (1994) 871-893.
6. N. M. Gallagher, A. Olankitwanit, A. Rajca, High-Spin Organic Molecules, J. Org. Chem. 80 (2015) 1291-1298.
7. M. Abe, Diradicals, Chem. Rev. 113 (2013) 7011-7088.
8. W. C. Lineberger, W. T. Borden, The synergy between qualitative theory, quantitative calculations, and direct experiments in understanding, calculating, and measuring the energy differences between the lowest singlet and triplet states of organic diradicals, Phys. Chem. Chem. Phys. 13 (2011) 11792-11813.
9. G. A. Zissimou, A. A. Berezin, M. Manoli, C. Nicolaides, T. Trypiniotis, P. A. Koutentis, 3,3′,3″-(Benzene-1,3,5-triyl)tris(1-phenyl-1*H*-benzo[*e*][1,2,4]triazin-4-yl): A C3 symmetrical Blatter-type triradical, Tetrahedron 76 (2020) 131077.
10. N. M. Gallagher, J. J. Bauer, M. Pink, S. Rajca, A. Rajca, High-Spin Organic Diradical with Robust Stability, J. Am. Chem. Soc. 138 (2016) 9377-9380.
11. N. M. Gallagher, H. Zhang, T. Junghoefer, E. Giangrisostomi, R. Ovsyannikov, M. Pink, S. Rajca, M. B. Casu, A. Rajca, Thermally and Magnetically Robust Triplet Ground State Diradical, J. Am. Chem. Soc. 141 (2019) 4764-4774.
12. C. Shu, M. Pink, T. Junghoefer, E. Nadler, S. Rajca, M. B. Casu, A. Rajca, Synthesis and Thin Films of Thermally Robust Quartet (S = 3/2) Ground State Triradical, J. Am. Chem. Soc. 143 (2021) 5508-5518.

13. S. Zhang, M. Pink, T. Junghoefer, W. Zhao, S.-N. Hsu, S. Rajca, A. Calzolari, B. W. Boudouris, M. B. Casu, A. Rajca, High-Spin (S = 1) Blatter-Based Diradical with Robust Stability and Electrical Conductivity, J. Am. Chem. Soc. 144 (2022) 6059-6070.
14. Y. Zhang, Y. Zheng, H. Zhou, M.-S. Miao, F. Wudl, T.-Q. Nguyen, Temperature Tunable Self-Doping in Stable Diradicaloid Thin-Film Devices, Adv. Mater. 27 (2015) 7412-7419.
15. X. Hu, H. Chen, G. Xue, Y. Zheng, Correlation between the strength of conjugation and spin–spin interactions in stable diradicaloids, J. Mater. Chem. C, 8 (2020) 10749-10754.
16. X. Hu, H. Chen, L. Zhao, M. Miao, J. Han, J. Wang, J. Guo, Y. Hu, Y. Zheng, Nitrogen analogues of Chichibabin's and Müller's hydrocarbons with small singlet–triplet energy gaps, Chem. Commun. 55 (2019) 7812-7815.
17. X. Hu, H. Chen, L. Zhao, M.-s. Miao, X. Zheng, Y. Zheng, Nitrogen-coupled blatter diradicals: the fused versus unfused bridges, J. Mater. Chem. C 7 (2019) 10460-10464.
18. H. M. Blatter, H. Lukaszewski, A new stable free radical, Tetrahedron Lett. 9 (1968) 2701-2705.
19. C. P. Constantinides, P. A. Koutentis, Stable N- and N/S-Rich Heterocyclic Radicals: Synthesis and Applications, Adv. Heterocycl. Chem. 119 (2016) 173-207.
20. Y. Ji, L. Long, Y. Zheng, Recent advances of stable Blatter radicals: synthesis, properties and applications, Mater. Chem. Front. 4 (2020) 3433-3443.
21. F. J. M. Rogers, P. L. Norcott, M. L. Coote., Recent advances in the chemistry of benzo[e][1,2,4]triazinyl radicals, Org. Biomol. Chem. 18 (2020) 8255-8277.
22. S. Kumar, Y. Kumar, S. K. Keshri, P. Mukhopadhyay, Recent Advances in Organic Radicals and Their Magnetism, Magnetochemistry 2 (2016) 42.

23. C. P. Constantinides, P. A. Koutentis, H. Krassos, J. M. Rawson, A. J. Tasiopoulos, Characterization and Magnetic Properties of a “Super Stable” Radical 1,3-Diphenyl-7-trifluoromethyl-1,4-dihydro-1,2,4-benzotriazin-4-yl, J. Org. Chem. 76 (2011) 2798-2806.
24. P. A. Koutentis, D. Lo Re, Catalytic Oxidation of N-Phenylamidrazones to 1,3-Diphenyl-1,4-dihydro-1,2,4-benzotriazin-4-yls: An Improved Synthesis of Blatter’s Radical, Synthesis 12 (2010) 2075-2079.
25. A. A. Berezin, C. P. Constantinides, S. I. Mirallai, M. Manoli, L. L. Cao, J. M. Rawson, P. A. Koutentis, Synthesis and properties of imidazolo-fused benzotriazinyl radicals, Org. Biomol. Chem. 11 (2013) 6780-6795.
26. A. A. Berezin, G. Zissimou, C. P. Constantinides, Y. Beldjoudi, J. M. Rawson, P. A. Koutentis, Route to Benzo- and Pyrido-Fused 1,2,4-Triazinyl Radicals via N′-(Het)aryl-N′-[2-nitro(het)aryl]hydrazides, J. Org. Chem. 79 (2014) 314-327.
27. A. C. Savva, S. I. Mirallai, G. A. Zissimou, A. A. Berezin, M. Demetriades, A. Kourtellaris, C. P. Constantinides, C. Nicolaides, T. Trypiniotis, P. A. Koutentis, Preparation of Blatter Radicals via Aza-Wittig Chemistry: The Reaction of N-Aryliminophosphoranes with 1-(Het)aroyl-2-aryldiazenes, J. Org. Chem. 82 (2017) 7564-7575.
28. A. A. Berezin, C. P. Constantinides, C. Drouza, M. Manoli, P. A. Koutentis, From Blatter Radical to 7-Substituted 1,3-Diphenyl-1,4-dihydrothiazolo[5′,4′:4,5]benzo[1,2-*e*][1,2,4]triazin-4-yls: Toward Multifunctional Materials, Org. Lett. 14 (2012) 5586-5589.
29. C. P. Constantinides, P. A. Koutentis, G. Loizou, Synthesis of 7-aryl/heteraryl-1,3-diphenyl-1,2,4-benzotriazinyls viapalladium catalyzed Stille and Suzuki-Miyaura reactions, Org. Biomol. Chem. 9 (2011) 3122-3125.

30. C. P. Constantinides, P. A. Koutentis, J. M. Rawson, Antiferromagnetic Interactions in 1D Heisenberg Linear Chains of 7-(4-Fluorophenyl) and 7-Phenyl-Substituted 1,3-Diphenyl-1,4-dihydro- 1,2,4-benzotriazin-4-yl Radicals, Chem. - Eur. J. 18 (2012) 15433-15438.
31. C. P. Constantinides, A. A. Berezin, M. Manoli, G. M. Leitus, G. A. Zissimou, M. Bendikov, J. M. Rawson, P. A. Koutentis, Structural, Magnetic, and Computational Correlations of Some Imidazolo-Fused 1,2,4-Benzotriazinyl Radicals, Chem. - Eur. J. 20 (2014) 5388-5396.
32. C. P. Constantinides, P. A. Koutentis, J. M. Rawson, Ferromagnetic Interactions in a 1D Alternating Linear Chain of π-Stacked 1,3-Diphenyl-7-(thien-2-yl)-1,4-dihydro-1,2,4-benzotriazin-4-yl Radicals, Chem. - Eur. J. 18 (2012) 7109-7116.
33. C. P. Constantinides, A. A. Berezin, M. Manoli, G. M. Leitus, M. Bendikov, J. M. Rawson, P. A. Koutentis, Effective exchange coupling in alternating-chains of a π-extended 1,2,4-benzotriazin-4-yl, New J. Chem. 38 (2014) 949-954.
34. C. P. Constantinides, A. A. Berezin, G. A. Zissimou, M. Manoli, G. M. Leitus, M. Bendikov, M. R. Probert, J. M. Rawson, P. A. Koutentis, A Magnetostructural Investigation of an Abrupt Spin Transition for 1-Phenyl-3-trifluoromethyl-1,4-dihydrobenzo[*e*][1,2,4]triazin-4-yl, J. Am. Chem. Soc. 136 (2014) 11906-11909.
35. C. P. Constantinides, E. Carter, D. M. Murphy, M. Manoli, G. M. Leitus, M. Bendikov, J. M. Rawson, P. A. Koutentis, Spin-triplet excitons in 1,3-diphenyl-7-(fur-2-yl)-1,4-dihydro-1,2,4-benzotriazin-4-yl, Chem. Commun. 49 (2013) 8662-8664.
36. C. P. Constantinides, A. A. Berezin, G. A. Zissimou, M. Manoli, G. M. Leitus, P. A. Koutentis, The Suppression of Columnar π-Stacking in 3-Adamantyl-1-phenyl-1,4-dihydrobenzo[*e*][1,2,4]triazin-4-yl, Molecules 21 (2016) 636 (1-7).

37. C. P. Constantinides, D. B. Lawson, A. A. Berezin, G. A. Zissimou, M. Manoli, G. M. Leitus, P. A. Koutentis, Ferromagnetic interactions in a 1D Heisenberg linear chain of 1-phenyl-3,7-bis(trifluoromethyl)-1,4-dihydro-1,2,4-benzotriazin-4-yls, CrystEngComm 21 (2019) 4599-4606.
38. F. Bazzi, A. J. Danke, D. B. Lawson, M. Manoli, G. M. Leitus, P. A. Koutentis, C. P. Constantinides, 1-(2-Methoxyphenyl)-3-phenyl-1,4-dihydro-1,2,4-benzotriazin-4-yl: a tricky “structure-to-magnetism” correlation aided by DFT calculations, CrystEngComm 22 (2020) 4306-4316.
39. C. P. Constantinides, D. B. Lawson, G. A. Zissimou, A. A. Berezin, A. Mailman, M. Manoli, A. Kourtellaris, G. M. Leitus, R. Clérac, H. M. Tuononen, P. A. Koutentis, Polymorphism in a π stacked Blatter radical: structures and magnetic properties of 3-(phenyl)-1-(pyrid-2-yl)-1,4-dihydrobenzo[*e*][1,2,4]triazin-4-yl, CrystEngComm 22 (2020) 5453-5463.
40. Y. Zhang, Y. Zheng, H. Zhou, M.-S. Miao, F. Wudl and T.-Q. Nguyen, Temperature Tunable Self-Doping in Stable Diradicaloid Thin-Film Devices, Adv. Mater. 27 (2015) 7412-7419.
41. Y. Zheng, M.-S. Miao, G. Dantelle, N. D. Eisenmenger, G. Wu, I. Yavuz., M. L. Chabinyc, K. N. Houk, F. Wudl, A Solid-State Effect Responsible for an Organic Quintet State at Room Temperature and Ambient Pressure, Adv. Mater. 27 (2015) 1718-1723.
42. M. Jasinski, S. Kapuscinski, P. Kaszynski, Stability of a columnar liquid crystalline phase in isomeric derivatives of the 1,4-dihydrobenzo[*e*][1,2,4]triazin-4-yl: Conformational effects in the core, J. Mol. Liq. 277 (2019) 1054-1059.

43. M. Jasinski, K. Szymanska, A. Gardias, D. Pociecha, H. Monobe, J. Szczytko, P. Kaszynski, Tuning the Magnetic Properties of Columnar Benzo[*e*][1,2,4]triazin-4-yls with the Molecular Shape, ChemPhysChem 20 (2019) 636-644.
44. S. Kapuscinski, A. Gardias, D. Pochiecha, M. Jasinski, J. Szczytko, P. Kaszynksi, Magnetic behaviour of bent-core mesogens derived from the 1,4-dihydrobenzo[*e*][1,2,4]triazin-4-yl, J. Mater. Chem. C 6 (2018) 3079-3088.
45. M. Jasinski, J. Szczytko, D. Pochiecha, H. Monobe, P. Kaszynski, Substituent-Dependent Magnetic Behavior of Discotic Benzo[*e*][1,2,4]triazinyls, J. Am. Chem. Soc. 138 (2016) 9421-9424.
46. B. Häupler, U. S. Schubert, A. Wild, P. A. Koutentis, G. Zissimou, Verwendung benzotriazinyl-haltiger Polymere als Ladungsspeicher, *DE Pat.*, 102017005924 (A1) 2018.
47. A. Saal, C. Friebe, U. S. Schubert, Blatter radical as a polymeric active material in organic batteries, J. Power Sources 524 (2022) 231061.
48. J. S. Steen, J. L. Nuismer, V. Eiva, A. E. T. Wiglema, N. Daub, J. Hjelm, E. Otten, Blatter Radicals as Bipolar Materials for Symmetrical Redox-Flow Batteries, J. Am. Chem. Soc. 144 (2022) 5051-5058.
49. I. S. Morgan, A. Peuronen, M. M. Hänninen, R. W. Reed, R. Clérac, H. M. Tuononen, 1-Phenyl-3-(pyrid-2-yl)benzo[*e*][1,2,4]triazinyl: The First “Blatter Radical” for Coordination Chemistry, Inorg. Chem. 53 (2014) 33-35.
50. I. S. Morgan, A. Mansikkamäki, G. A. Loizou, P. A. Koutentis, M. Rouzières, R. Clérac, H. M. Tuononen, Coordination Complexes of a Neutral 1,2,4-Benzotriazinyl Radical

Ligand: Synthesis, Molecular and Electronic Structures, and Magnetic Properties, Chem. - Eur. J. 21 (2015) 15843-15853.

51. I. S. Morgan, A. Mansikkamäki, M. Rouzières, R. Clérac, H. M. Tuononen, Coexistence of long-range antiferromagnetic order and slow relaxation of the magnetization in the first lanthanide complex of a 1,2,4-benzotriazinyl radical, Dalton Trans. 46 (2017) 12790-12793.
52. A. S. Poryvaev, D. M. Polyukhov, E. Gjuzi, F. Hoffmann, M. Fröba, M.V. Fedin, Radical-Doped Metal–Organic Framework: Route to Nanoscale Defects and Magnetostructural Functionalities, Inorg. Chem. 58 (2019) 8471-9479.
53. M. Demetriou, A. A. Berezin, P. A. Koutentis, T. Krasia-Christoforou, Benzotriazinyl-mediated controlled radical polymerization of styrene, Polym. Int. 63 (2014) 674-679.
54. J. Areephong, K. M. Mattson, N. J. Treat, S. O. Poelma, J. W. Kramer, H. A. Sprafke, A. A. Latimer, J. Read de Alaniz, C. J. Hawker, Triazine-mediated controlled radical polymerization: new unimolecular initiators, Polym. Chem. 7 (2016) 370-374.
55. J. Areephong, N. Treat, J. W. Kramer, M. D. Christianson, H. A. Collins, Triazine mediated living radical controlled polymerization, 2016 US 0311785 A1.
56. F. J. M. Rogers, M. L. Coote, Computational Evaluation of the Oxidative Cleavage of Triazine Derivatives for Electrosynthesis, J. Phys. Chem. C 123 (2019) 10306-10310.
57. F. A. Perras, D. F. Flesariu, S. A. Southern, C. Nicolaides, J. D. Bazak, N. M. Washton, T. Trypiniotis, C. P. Constantinides, P. A. Koutentis, Methyl-Driven Overhauser Dynamic Nuclear Polarization, J. Phys. Chem. Lett. 13 (2022) 4000-4006.
58. Y. Zheng, M.-s. Miao, M. C. Kemei, R. Seshadri, F. Wudl, The Pyreno-Triazinyl Radical – Magnetic and Sensor Properties, Isr. J. Chem. 54 (2014) 774-778.

59. F. Ciccullo, N. M. Gallagher, O. Geladari, T. Chassé, A. Rajca, M. B. Casu, A Derivative of the Blatter Radical as a Potential Metal-Free Magnet for Stable Thin Films and Interfaces, ACS Appl. Mater. Interfaces 8 (2016) 1805-1812.
60. M. B. Casu, Nanoscale Studies of Organic Radicals: Surface, Interface, and Spinterface, Acc. Chem. Res. 51 (2018) 753-760.
61. J. Z. Low, G. Kladnik, L. L. Patera, S. Sokolov, G. Lovat, E. Kumarasamy, J. Repp, L. M. Campos, D. Cvetko, A. Morgante, L. Venkataraman, The Environment-Dependent Behavior of the Blatter Radical at the Metal–Molecule Interface, Nano Lett. 19 (2019) 2543-2548.
62. L. L. Patera, S. Sokolov, J. Low, L. Campos, L. Venkataraman, J. Repp, Resolving the Unpaired-Electron Orbital Distribution in a Stable Organic Radical by Kondo Resonance Mapping, Angew. Chem. Int. Ed. 131 (2019) 11179-11183.
63. F. Ciccullo, A. Calzolari, K. Bader, P. Neugebauer, N. M. Gallagher, A. Rajca, J. van Slageren, M. B. Casu, Interfacing a Potential Purely Organic Molecular Quantum Bit with a Real-Life Surface, ACS Appl. Mater. Interfaces 11 (2019) 1571-1578.
64. CrysAlis CCD and CrysAlis RED, version 1.171.32.15; Oxford Diffraction Ltd, Abingdon, Oxford, England, 2008.
65. Sheldrick, G. M. SHELXL-97: A program for the refinement of crystal structure; University of Göttingen: Göttingen, Germany, 1997.
66. L. Farrugia, WinGX suite for small-molecule single-crystal crystallography, J. Appl. Cryst. 32 (1999) 837–838.
67. Brandenburg, K. DIAMOND, version 3.1d; Crystal Impact GbR, Bonn, Germany, 2006.

68. S. Stoll, A. Schweiger, EasySpin, a comprehensive software package for spectral simulation and analysis in EPR, J. Magn. Reson.178 (2006) 42-55.
69. A. D. Becke, Density-functional thermochemistry. III. The role of exact exchange, J. Chem. Phys. 98 (1993) 5648-5652.
70. C. Lee, W. Yang, R. G. Parr, Development of the Colle-Salvetti correlation-energy formula into a functional of the electron density, Phys. Rev. B 37 (1988) 785-789.
71. S.H. Vosko, L. Wilk, M. Nusair, Accurate spin-dependent electron liquid correlation energies for local spin density calculations: a critical analysis, Can. J. Phys. 58 (1980) 1200-1211.
72. P. J. Stephens, F. J. Devlin, C. F. Chabalowski, M. J. Frisch, Ab Initio Calculation of Vibrational Absorption and Circular Dichroism Spectra Using Density Functional Force Fields, J. Phys. Chem. 98 (1994) 11623-11627.
73. F. Weigenda, R. Ahlrichs, Balanced basis sets of split valence, triple zeta valence and quadruple zeta valence quality for H to Rn: Design and assessment of accuracy, Phys. Chem. Chem. Phys. 7 (2005) 3297-3305.
74. Gaussian 16, Revision C.01, M. J. Frisch, G. W. Trucks, H. B. Schlegel, G. E. Scuseria, M. A. Robb, J. R. Cheeseman, G. Scalmani, V. Barone, G. A. Petersson, H. Nakatsuji, X. Li, M. Caricato, A. V. Marenich, J. Bloino, B. G. Janesko, R. Gomperts, B. Mennucci, H. P. Hratchian, J. V. Ortiz, A. F. Izmaylov, J. L. Sonnenberg, D. Williams-Young, F. Ding, F. Lipparini, F. Egidi, J. Goings, B. Peng, A. Petrone, T. Henderson, D. Ranasinghe, V. G. Zakrzewski, J. Gao, N. Rega, G. Zheng, W. Liang, M. Hada, M. Ehara, K. Toyota, R. Fukuda, J. Hasegawa, M. Ishida, T. Nakajima, Y. Honda, O. Kitao, H. Nakai, T. Vreven, K. Throssell, J. A. Montgomery, Jr., J. E. Peralta, F. Ogliaro, M. J. Bearpark, J. J. Heyd,

E. N. Brothers, K. N. Kudin, V. N. Staroverov, T. A. Keith, R. Kobayashi, J. Normand, K. Raghavachari, A. P. Rendell, J. C. Burant, S. S. Iyengar, J. Tomasi, M. Cossi, J. M. Millam, M. Klene, C. Adamo, R. Cammi, J. W. Ochterski, R. L. Martin, K. Morokuma, O. Farkas, J. B. Foresman, and D. J. Fox, Gaussian, Inc., Wallingford CT, 2016.

75. K. Kambe, On the Paramagnetic Susceptibilities of Some Polynuclear Complex Salts, J. Phys. Soc. Jpn. 5 (1950) 48-51.
76. D. Reta, I. de P. R. Moreira, F. Illas, Magnetic Coupling Constants in Three Electrons Three Centers Problems from Effective Hamiltonian Theory and Validation of Broken Symmetry-Based Approaches, J. Chem. Theory and Comput. 12 (2016) 3228-3235.
77. L. Mathivathanan, G. Rogez, N. B. Amor, V. Robert, R. G. Raptis, A. K. Boudalis, Origin of Ferromagnetism and Magnetic Anisotropy in a Family of Copper(II) Triangles, Chem. - Eur. J. 26 (2020) 12769-12784.
78. S. S. Eaton, L. B. Woodcock, G. R. Eaton, Continuous wave electron paramagnetic resonance of nitroxide biradicals in fluid solution, Concepts Magn Reson Part A, 47A (2018) e21426.
79. M. Weger, Passage Effects in Paramagnetic Resonance Experiments, Bell Syst. Tech. J. 39 (1960) 1013-1112.
80. Eaton, S. S.; Eaton, G. R. Electron Paramagnetic Resonance. In *Ewing's analytical instrumentation handbook*; Cazes, J., Ewing, G. W., Eds.; Marcel Dekker: New York, 2005 349–398.